

solarFLAG hare and hounds: estimation of p-mode frequencies from Sun-as-star helioseismology data

S. J. Jiménez-Reyes^{1,2*}, W. J. Chaplin^{2,†}, R. A. García³, T. Appourchaux⁴,
F. Baudin⁴, P. Boumier⁴, Y. Elsworth², S. T. Fletcher⁵, M. Lazrek^{6,7,8},
J. W. Leibacher^{9,4}, J. Lochard¹, R. New⁵, C. Régulo^{1,10}, D. Salabert^{1,9},
T. Toutain², G. A. Verner^{11,2} and R. Wachter¹²

¹ Instituto de Astrofísica de Canarias, 38205, La Laguna, Tenerife, Spain

² School of Physics and Astronomy, University of Birmingham, Edgbaston, Birmingham, B15 2TT, UK

³ Laboratoire AIM, CEA/DSM-CNRS-Université Paris Diderot; CEA-Saclay, IRFU, SAp, F-91191, Gif-sur-Yvette, France

⁴ Institut d'Astrophysique Spatiale (IAS), Bâtiment 121, F-91405, Orsay Cedex, France

⁵ Faculty of Arts, Computing, Engineering and Sciences, Sheffield Hallam University, Sheffield S1 1WB, UK

⁶ LPHEA, Faculté des Sciences Semlalia, Université Cadi Ayyad, Marrakech, Morocco

⁷ Département d'Astrophysique, UMR 6525, Université de Nice-Sophia Antipolis, 06108 Nice Cedex 2, France

⁸ Département Cassini, URA CNRS 1362, Observatoire de la Côte d'Azur, F-06304 Nice, France

⁹ National Solar Observatory, 950 North Cherry Avenue, Tucson, AZ 85719, USA

¹⁰ Dpto. de Astrofísica, Universidad de La Laguna, La Laguna, 38206, Tenerife, Spain

¹¹ Astronomy Unit, Queen Mary, University of London, Mile End Road, London, E1 4NS, UK

¹² W. W. Hansen Experimental Physics Laboratory, Stanford University, Stanford, CA 94305-4085

5 November 2018

ABSTRACT

We report on the results of the latest solarFLAG hare-and-hounds exercise, which was concerned with testing methods for extraction of frequencies of low-degree solar p modes from data collected by Sun-as-a-star observations. We have used the new solarFLAG simulator, which includes the effects of correlated mode excitation and correlations with background noise, to make artificial timeseries data that mimic Doppler velocity observations of the Sun as a star. The correlations give rise to asymmetry of mode peaks in the frequency power spectrum. Ten members of the group (the hounds) applied their “peak bagging” codes to a 3456-day dataset, and the estimated mode frequencies were returned to the hare (who was WJC) for comparison. Analysis of the results reveals a systematic bias in the estimated frequencies of modes above ≈ 1.8 mHz. The bias is negative, meaning the estimated frequencies systematically underestimate the input frequencies.

We identify two sources that are the dominant contributions to the frequency bias. Both sources involve failure to model accurately subtle aspects of the observed power spectral density in the part (window) of the frequency power spectrum that is being fitted. One source of bias arises from a failure to account for the power spectral density coming from all those modes whose frequencies lie outside the fitting windows. The other source arises from a failure to account for the power spectral density of the weak $l = 4$ and 5 modes, which are often ignored in Sun-as-a-star analysis. The Sun-as-a-star peak-bagging codes need to allow for both sources, otherwise the frequencies are likely to be biased.

Key words:

Sun: helioseismology – Sun: interior – methods: data analysis

1 INTRODUCTION

The solar Fitting at Low-Angular degree Group (*solarFLAG*)¹ has as its main aims the development and refinement of techniques for

* E-mail: sjimenez@ll.iac.es

† E-mail: w.j.chaplin@bham.ac.uk

analysis of data from the low-degree (low- l) p modes, from observations made of the “Sun as a star”. These data play a crucial rôle in studies of the deep radiative interior and core of the Sun.

The input data for probing the solar interior are the mode parameters, such as individual frequencies, frequency splittings, damping rates and powers. The mode frequencies may be used to infer the internal hydrostatic structure (sound speed, density); accurate and precise frequencies are a vital prerequisite for ensuring that robust inference is made on the structure.

Analysis of the Sun-as-a-star (and also the resolved-Sun) helioseismic data requires application of complicated algorithms to extract estimates of the mode parameters. This usually involves fitting multi-parameter models to the resonant peaks in the frequency power spectrum of the observations. An important aim of the solarFLAG program is to quantify levels of bias arising from, and precision achievable in, these *peak bagging* procedures. “Hare and hounds” exercises on realistic artificial data form the framework for this activity.

In a first study (Chaplin et al. 2006) we looked in detail at the accuracy and precision of rotational frequency splittings extracted from a 3456-d set of artificial Sun-as-a-star data, to which ten members of the solarFLAG applied their peak-bagging codes. The parameters we look at in this paper are the low- l mode frequencies returned by the peak-bagging codes. The sets of artificial timeseries data used in our first study did not include any asymmetry of the simulated p-mode peaks in the frequency power spectrum; this asymmetry is exhibited by the real solar p modes. The peak-bagging codes must be able to cope with the asymmetry to in principle allow accurate estimation of the mode frequencies. It was therefore clear to us that to expedite a meaningful hare-and-hounds study on the mode frequencies we would need to generate artificial data with asymmetry included. This we have now done, and this paper reports on results of a hare-and-hounds exercise conducted with the new asymmetric artificial data, to which ten members of the solarFLAG applied their peak-bagging codes.

We have used a simple, but very powerful method to introduce in the time domain the effects of asymmetry, which is based on the framework proposed by Toutain, Elsworth & Chaplin (2006). There are two main factors in the method that contribute to the asymmetry of the artificial mode peaks. First, background noise is correlated with the excitation functions of the modes. Second, overtones of the same angular degree and azimuthal order have excitation functions that are correlated in time (see Chaplin, Elsworth & Toutain 2008). In this framework, correlation of the excitation follows naturally from invoking correlations with the background noise. As we shall see in this paper, the power spectral density of the resulting asymmetric mode peaks must be modelled accurately, otherwise estimates of the mode frequencies returned by the peak-bagging codes will be biased. This is the main result of the paper.

The layout of the rest of the paper is as follows. Section 2 gives a brief overview of the solarFLAG simulator, which was used to make the artificial timeseries data for the hare-and-hounds exercise. We also discuss in this section the basic attributes of the artificial dataset analyzed by the ten hounds. A detailed description of the simulator, which pays particular attention to the impact of correlations in the data, is given in Chaplin et al. (in preparation).

Section 3 summarizes the main elements of the fitting strategies that were adopted by the hounds. Section 4 then presents the main results of the hare-and-hounds exercise. We look in detail at how the estimated frequencies of the hounds compared, not only against the input frequencies (results which bear on the accuracy of the peak-bagging procedures), but also against one another (results

which bear on the precision inherent in the estimated frequencies). In Section 5 we identify the origins of a systematic frequency bias that is reported in Section 4. Finally, we conclude in Section 6 with a summary of the main conclusions of the paper, where we also discuss implications of the frequency bias for the fitting strategies.

2 THE SOLARFLAG SIMULATOR

2.1 General information

The solarFLAG datasets simulate full-disc Sun-as-a-star Doppler velocity observations, such as those made by the ground-based Birmingham Solar-Oscillations Network (BiSON) and the Global Oscillations at Low-Frequency (GOLF) instrument on board the *ESA/NASA* SOHO spacecraft. The dataset made by the hare (who was WJC) for the hare-and-hounds exercise spanned 3456 simulated days, with data samples made on a regular 40-sec cadence. The dataset did not include any solar-cycle effects. The impact of these effects will be dealt with in a separate paper.

solarFLAG datasets are made with a full complement of simulated low- l modes. The hare-and-hounds dataset included all modes in the ranges $0 \leq l \leq 5$ and $1000 \leq \nu \leq 5000 \mu\text{Hz}$. Frequencies of the modes came from standard solar model BS05(OP) of Bahcall et al. (2005). We also added a surface term to these frequencies, which was based on polynomial fits to differences between the raw model BS05(OP) frequencies and frequencies from analysis of BiSON and GOLF data. A database of p-mode power, linewidth and peak asymmetry estimates, obtained from analyses of GOLF and BiSON data, was used to guide the choice of the other input mode parameters.

The hypothetical solarFLAG instrument was assumed to make its observations from a location in, or close to, the ecliptic plane. This is the perspective from which BiSON (ground-based network) and GOLF (orbiting the Sun at the L1 Lagrangian point) view the Sun. The rotation axis of the Sun is then always nearly perpendicular to the line-of-sight direction, and only a subset of the $2l + 1$ components of the non-radial modes are clearly visible: those having even $l + m$, where m is the azimuthal order. These components are represented explicitly in the solarFLAG timeseries. The visibility for given (l, m) also depends, though to a lesser extent, on the spatial filter of the instrument (e.g., see Christensen-Dalsgaard 1989). Here, we adopted BiSON-like visibility ratios.

We included two sources of background noise in the data, which have a significant power contribution in the range occupied by the p modes. First, a simple photon shot noise component, having a white frequency power spectrum. This component was made in the time domain from random Gaussian noise, specified by a sample standard deviation of $\sigma_{\text{psn}} = 0.25 \text{ m s}^{-1}$ per 40-sec sample. The other source of background was granulation-like noise, having a frequency power spectrum like the Harvey (1985) power-law model. As we shall see below – where we also specify its basic parameters – this noise is used to excite the modes, and plays a crucial rôle in the correlations introduced in the data.

2.2 Correlated excitation and correlated noise

The solarFLAG simulator models the effects of correlated mode excitation and correlated background noise. One does not need to understand the detail of the implementation in order to follow the discussion of the results in this paper. Rather, one needs only to

take away the two following, key points: First, inclusion of correlation effects gives rise to asymmetric peaks in the frequency power spectrum; and these correlations may be tuned in the simulator to give asymmetries which resemble closely those displayed in real Sun-as-a-star data. Second, the impact of the correlations is such that the power spectral density in the outlying tails of the mode peaks falls off in a manner that is evidently similar to that in the real data. Frequency power spectra of full solarFLAG timeseries therefore show a close resemblance, in their overall appearance, to real Sun-as-a-star spectra. We considered these two points as important baseline requirements for any artificial dataset used in the hare-and-hounds exercises.

An in-depth discussion of the implementation of the correlations, and full details on the simulator, are given in Chaplin et al. (in preparation). In what remains of this section we give a summary of the basic principles, and a brief overview of the simulator. We also show the underlying peak asymmetries that were introduced in the solarFLAG hare-and-hounds dataset.

2.2.1 Basic principles

In Toutain, Elsworth & Chaplin (2006) it was hypothesized that the excitation function of an overtone, n , with angular degree l and azimuthal degree m (whose frequency is ν_{nlm}), is the same as that component of the solar background (granulation) noise that has the same spherical harmonic projection, Y_{lm} , in the corresponding range in frequency in the Fourier domain. An important implication is that overtones with the same (l, m) should have excitation functions that are correlated in time. (Note that the Y_{lm} for (l, m) and $(l, -m)$ are orthogonal, and are therefore assumed to have independent, i.e., uncorrelated, excitation.) Moreover, since Doppler velocity observations of the Sun are also sensitive to the granulation background, perturbations due to the modes and this noise will be correlated in time. This is what we call correlated background noise (see also, e.g., Roxburgh & Vorontsov 1997; Severino et al. 2001; Gabriel et al. 2001; Jefferies et al. 2003; Barban, Hill & Kras 2004; and references therein).

Even in the absence of any correlated background noise, the correlated excitation would give rise to asymmetry of mode peaks in the frequency power spectrum. This asymmetry is due to complex interactions between the tails of the correlated mode peaks. When the correlated background noise is included, there are then additional contributions to the peak asymmetry.

2.2.2 Inclusion of correlation effects in the simulator

The basis of the solarFLAG simulator is the method discussed in Chaplin et al. (1997) for generating timeseries of individual p modes. The method uses the Laplace transform solution of the equation of a forced, damped harmonic oscillator to make the output velocity of each artificial mode. Oscillators are re-excited at each time sample – the chosen cadence here being 40 sec – with small ‘kicks’ from a timeseries of random noise.

The kicks are drawn from a timeseries of granulation-like noise. This noise is made by using random white-noise input to a low-order, autoregressive model. Overtones of a given (l, m) have kicks that are correlated in time. The granulation-like noise is also used to give the correlated background noise. The granulation-like noise is specified by two free parameters: σ fixes the amplitude; while the characteristic timescale, τ , is given a value to mimic the lifetime of granules on the Sun.

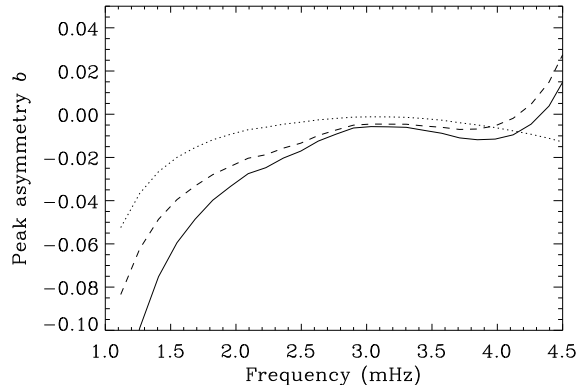


Figure 1. Peak asymmetry in the solarFLAG hare-and-hounds dataset. Thick solid line: total asymmetry. Dotted line: contribution due to correlated background noise. Dashed line: contribution due to correlated mode excitation.

A single constant, ρ , fixes the coefficient of correlation for the correlated excitation, and the correlation with the background (see also Chaplin, Elsworth & Toutain 2008). This gives the user the flexibility to ‘tune’ the asymmetry of the mode peaks – the higher is ρ , the larger is the asymmetry. When $\rho = \pm 1$, overtones with the same (l, m) are all excited by the same timeseries; when $\rho = 0$, they are excited by statistically independent timeseries; and when $0 < |\rho| < 1$ they are kicked by a mixture of common and independent timeseries. The common timeseries (or a mixture of common and independent timeseries data) is later added as background noise (having been suitably scaled in amplitude first).

Fig. 1 shows the input asymmetry given to mode peaks in the hare-and-hounds dataset. We note that the solarFLAG simulator was configured on the assumption that at a given frequency the relative sizes of the granulation noise and the mode amplitudes are independent of degrees l and m . An important consequence of this assumption is that, at a given frequency, the asymmetry contribution from the correlated noise – shown here as the dotted line – is the same for all (l, m) . This contribution is fixed for a given mode by three free parameters, the p-mode parameters (i.e., frequencies, heights, linewidths) having already been fully specified on input. The free parameters are: ρ , σ and τ . The hare-and-hounds timeseries was made with $\sigma = 0.2 \text{ m s}^{-1}$ and $\tau = 260 \text{ sec}$. The hare also settled on $\rho = -0.36$. Use of negative ρ gave negative peak asymmetry, as displayed in real Sun-as-a-star data; while the absolute value of ρ gave asymmetry that matched reasonably well that seen in BiSON and GOLF data.

The dashed line in Fig. 1 shows the contribution to the peak asymmetry arising from the correlated excitation. This contribution is fixed by the frequency separations, linewidths and relative heights of the overtones, and the choice of ρ . Since these mode parameters are similar for all (l, m) , so too are the peak asymmetries from this contribution (the figure shows the contribution for overtones of $l = 0$). Again, full details on all of the above are given in Chaplin et al. (in preparation).

The solid line in Fig. 1 shows the total input asymmetry for the hare-and-hounds solarFLAG dataset, given by the combined effect of the correlated noise and correlated excitation². This is the asym-

² There is actually a third contribution to the peak asymmetry, from the non-white frequency response of the excitation. The response in the vicin-

metry actually displayed by peaks in the frequency power spectrum, and is the asymmetry the hounds would aim to recover when fitting the asymmetry as a free parameter.

3 FITTING STRATEGIES OF THE HOUNDS

Ten members of the solarFLAG acted as hounds. They applied their peak-bagging codes to the frequency power spectrum of the complete hare-and-hounds dataset to recover estimates of the artificial mode frequencies. The ten hounds were: PB, STF, RAG, SJJ-R, ML, JL, DS, TT, GAV and RW. A priori information given to the hounds was limited to: the cadence and length of the timeseries; and the calibration and format of the stored residuals. For the purposes of this study we chose not to impose an observational window function on the timeseries (e.g., that from a ground-based network). This meant parameter extraction was tested under the more favourable conditions afforded by a 100-per-cent duty cycle.

All hounds adopted a peak-bagging approach to the analysis. We refer the reader back to Chaplin et al. (2006) for more details. Peak-bagging involves maximum-likelihood fitting of mode peaks in the frequency power spectrum to multi-parameter fitting models, where individual mode peaks are represented by Lorentzian-like functions. Here, all hounds used the asymmetric Lorentzian-like formula of Nigam & Kosovichev (1998) to model individual peaks.

A common peak-bagging strategy is to go through the frequency power spectrum fitting a mode pair at a time (the so-called “pair-by-pair” approach). This is because the $l = 0$ modes lie in close proximity in frequency to the $l = 2$ modes. The same is true for the $l = 1$ and $l = 3$ modes. Eight hounds used this standard approach, isolating narrow frequency windows, centred on the target pairs, to perform the fitting. Chosen window sizes varied from 40 to 50 μHz for the even- l pairs, and 40 to 60 μHz for the odd- l pairs.

In the standard approach the fitting models usually only include power from the target pair. They also use a flat offset to represent the pseudo-white background (which varies only very slowly with frequency in the range of interest). However, the models then fail to account for power spectral density in the fitting window that comes from two other sources: (i) the nearby, weak $l = 4$ and 5 peaks; and (ii), the slowly-decaying tails of the other even and odd- l pairs in the spectrum, whose resonant frequencies lie outside the fitting window.

The first of these sources is a bigger cause for concern where results on the even- l pairs are concerned, since the $l = 4$ and 5 modes usually lie in their fitting windows (e.g., see Fig. 8 of Chaplin et al., 2006). This is not usually the case for the odd- l pairs. A few hounds submitted results that allowed for the presence of the $l = 4$ and 5 modes.

A way around problems caused by the second source is of course to take account of the outlying power (e.g., see Jimenez, Roca-Cortés & Jimenez-Reyes 2002; Gelly et al. 2002; Fletcher et al. 2008), or to fit all modes in the frequency power spectrum in one go (e.g., see Lazrek et al. 2000; Appourchoux 2003). Two hounds also submitted results where they allowed for the outlying power in their fitting models. However, they did so by modelling the tails of the outlying peaks as symmetric Lorentzians, not the asymmetric functions actually displayed in the frequency power spectrum.

ity of each resonance of course rises with decreasing frequency, meaning there will be a small negative asymmetry contribution. This contribution is, however, very small compared to the contributions from correlated noise and correlated excitation.

As we shall see in Section 5, failure to deal properly with sources (i) and (ii) leads to bias in the estimated frequencies, and this dominates the other potential sources of bias. An example of another candidate source was use of inaccurate mode-component visibilities when modelling $l = 2$ and 3 multiplets during peak-bagging. In our first solarFLAG study (Chaplin et al., 2006), we showed that this was a major source of bias for estimation of the rotational frequency splittings. The frequencies are in contrast remarkably insensitive to the choice of the visibilities. There were differences in the numbers of parameters the hounds sought to estimate by fitting, and we also checked whether these differences could have affected the frequencies. One example was a division between those hounds who constrained the widths of all components in both modes of a pair to be the same (again, common practice at low l); and those who instead fitted two widths, one for each mode. This strategy did not have a significant impact on the estimated frequencies.

4 RESULTS

The main results of the hare-and-hounds exercise are shown in Figs. 2 and 3.

The results in Fig. 2 bear on the accuracy of the fitted frequencies. The four left-hand panels of this figure plot differences between the fitted and input frequencies (in the sense fitted minus input) at each degree, l . A different symbol is used to illustrate the results of each hound. In order to give a direct measure of the significance of these frequency differences, we divided the differences by the estimated frequency uncertainties. All hounds estimated uncertainties in the same way, taking, for each fit, the square root of the appropriate diagonal element of the inverted Hessian fitting matrix. The resulting normalized frequency differences (units of sigma) are plotted in the four right-hand panels of Fig. 2. The dot-dashed lines, which mark the $\pm 3\sigma$ -levels, are included as eye guides.

What conclusions may we draw from the results in Fig. 2? While at the lowest frequencies agreement between the fitted and input frequencies is very good, over most of the fitting range there is a persistent negative bias in the fitted frequencies. The significance of this bias reaches $\approx 3\sigma$ for some of the modes, and is largest at $l = 0$ (e.g., see the $l = 0$ results near ≈ 2.6 mHz). It is striking how the results of the different hounds follow one another quite closely at frequencies below ≈ 3.1 mHz. This reflects the fact that all fits are affected by the same realization noise. However, we shall show below in Section 5 that the negative bias *is not* simply a consequence of the realization noise, and that fitting results on timeseries made with the same input parameters, but different realization noise, also show negative bias.

At high frequencies the fitted frequencies are more scattered. In this part of the p-mode spectrum, large linewidths (high damping rates) cause nearby peaks to overlap in frequency. This happens not only within individual multiplets, where the effect becomes important above ≈ 3 mHz in the closely spaced $l = 1$ multiplets, but also between adjacent modes in the low- l pairs, where the effect becomes important above ≈ 3.5 mHz for even- l pairs (and at higher frequencies for the more widely separated odd- l pairs).

Next, let us consider differences *between* the hounds. These differences bear on the precision of the results. That is because disagreements in the results of fitting the same dataset imply the frequencies are not as precisely (or, for that matter, accurately) known as we might otherwise think. Disagreement in the results may be thought of as an additional source of uncertainty for the estimated

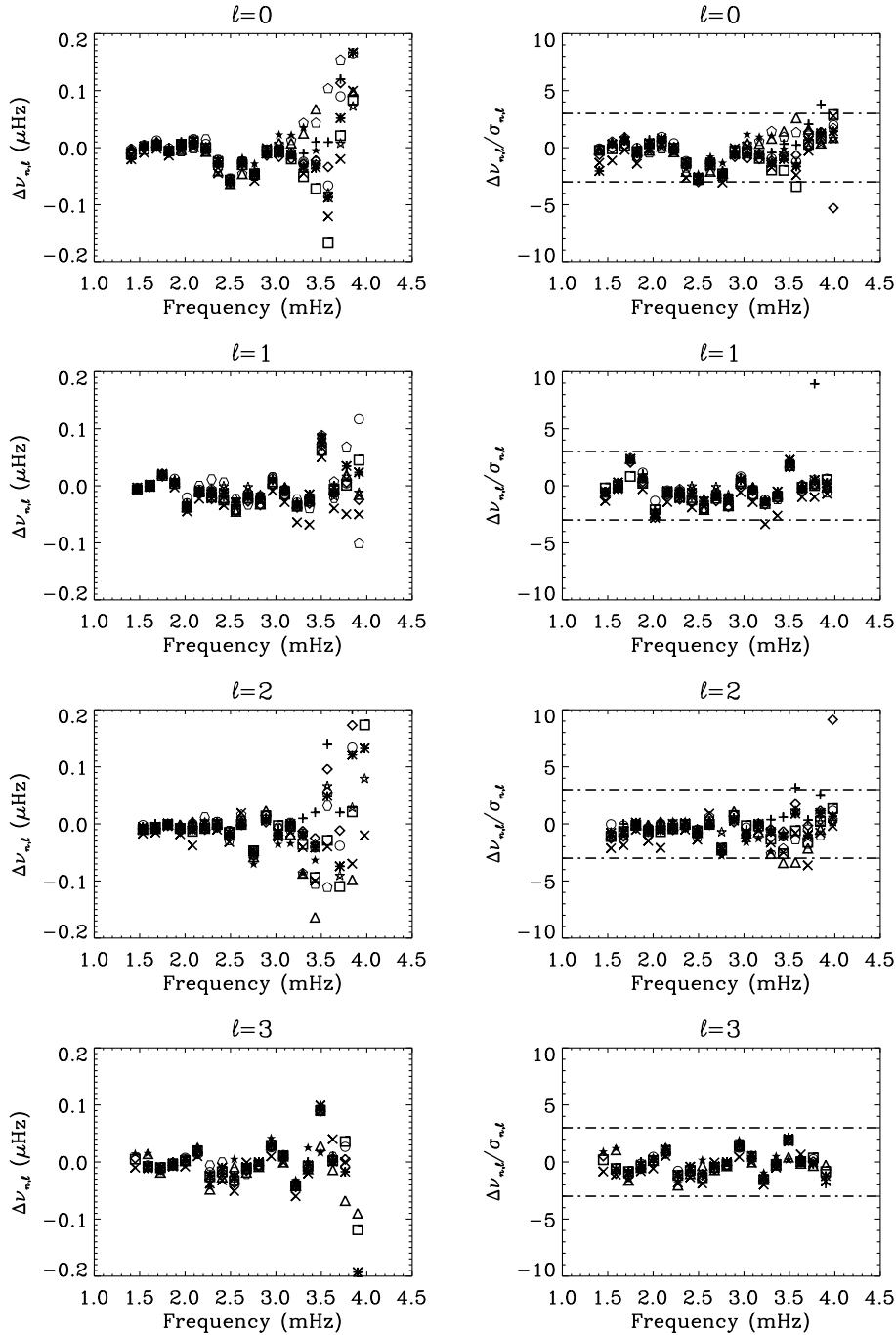


Figure 2. Left-hand panels: differences between the fitted and input frequencies (in the sense fitted minus input) at each degree, l (different symbol for each hound). Right-hand panels: Differences in the left-hand panels normalized by the estimated frequency uncertainties, to give differences in units of sigma. The dot-dashed lines mark the $\pm 3\sigma$ levels.

frequencies, over and above that due to the stochastic excitation and finite signal-to-noise ratio of the data.

This extra source of error – often referred to as reduction noise – may be estimated as follows. For each mode we calculated an RMS frequency difference of the fitted frequencies of the hounds, and then normalized that difference by the average of the hounds’ uncertainties for that mode, to give the normalized RMS differences plotted in Fig. 3 (units of sigma).

When the normalized RMS differences are close to zero, we may infer that agreement between the hounds is excellent. How-

ever, the results in Fig. 3 indicate this is clearly not the case for many of the fitted modes, where the normalized RMS differences are comparable to, or even larger in size than, the fitting uncertainties (i.e., the 1σ level). In order to get a measure of the typical size of this extra uncertainty, we computed histograms of the normalized RMS differences at each degree, l . These histograms are displayed as an inset to each panel of Fig. 3. The annotation also shows the standard deviations of the best-fitting Gaussian profiles of each histogram, which are in all cases comparable in size to 1σ . We conclude that reduction noise, arising from differences between

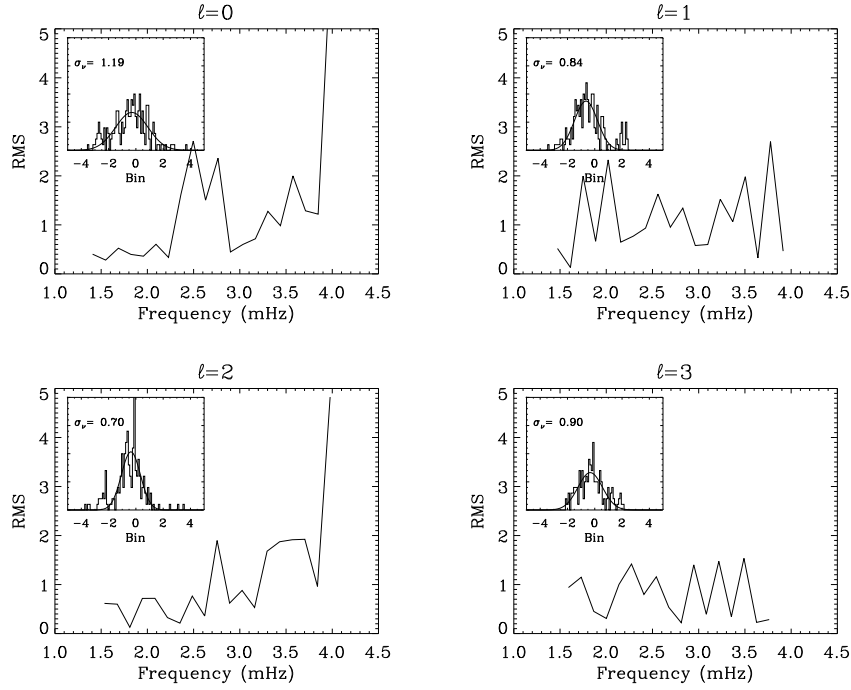


Figure 3. The curves in each panel show the RMS frequency differences, normalized by the mean of the fitting uncertainties returned by the hounds. These differences are referred to as normalized RMS differences in the text. Insets show histograms of the normalized RMS differences at each degree, l .

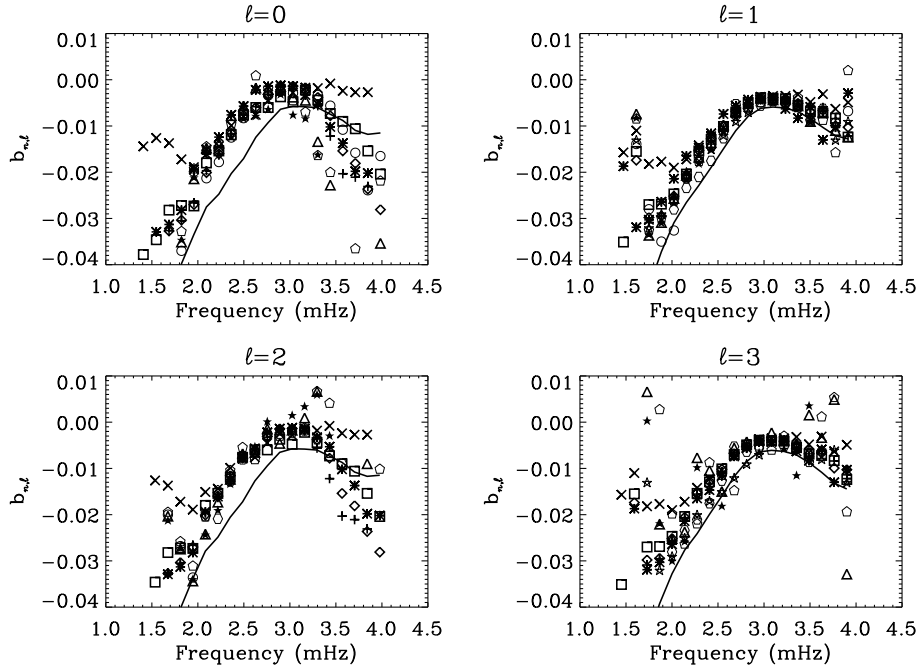


Figure 4. The estimated peak asymmetries (different symbol for each hound). The solid line in each panel is the input asymmetry.

the hounds, constitutes a significant source of uncertainty for the estimated frequencies.

Finally in this section, we also look at results on the fitted peak asymmetries. Poor estimation of the asymmetries will bias the fitted frequencies, and so results on the asymmetries are of considerable interest. Fig. 4 shows the fitted asymmetries of the hounds. The solid line in each panel is the input asymmetry (also shown as the solid line in Fig. 1). It is evident that several poor estimates of

the asymmetry were returned at the lowest frequencies. Here, the height-to-background ratio of the peaks takes its smallest values in the spectrum, and the peaks are also very narrow, making determination of the asymmetry less straightforward than in the main part of the spectrum. At the highest frequencies, the overlap of peaks also presents difficulties for the analysis. However, the most striking aspect of Fig. 4 is the persistent bias present in the estimates over the main part of the spectrum, where the returned estimates

systematically underestimate the actual input size of the asymmetry. We turn next to a detailed discussion of the bias.

5 DISCUSSION OF RESULTS

It turns out that two sources give a significant contribution to the bias in the frequencies shown in Section 4. Both sources, which were noted previously in Section 3, involve failure to model accurately subtle aspects of the observed power spectral density in the fitting windows. Again, they are: (i) power from $l = 4$ and 5 modes, which affects fits to the even- l pairs; and (ii) power from the slowly-decaying tails of the other even and odd- l pairs in the spectrum, whose resonant frequencies lie outside the fitting windows. In order to show clearly the bias from both of these sources, and to thereby explain the results from Section 4, we present here additional peak-bagging results. These results come from fits made to many independent realizations of artificial solarFLAG datasets. These datasets were identical, or similar, to the hare-and-hounds dataset.

The hare made four sequences of data. Each sequence was comprised of 25 independent realizations of the same artificial Sun. The four artificial suns defining each sequence had the same mode parameter, granulation noise and shot noise characteristics as the hare-and-hounds dataset. However, the coefficient describing the correlation of the excitation and noise background, and the number of degrees l in the data, was varied from one sequence to another. The content of the four sequences may be summarized as follows:

Sequence #1 — Datasets in this sequence were comprised of modes from $l = 0$ to 3, but there were *no* $l = 4$ and 5 modes. Furthermore, the excitation of the modes was uncorrelated; this meant there was also no correlation with the granulation-like noise background. The coefficient of correlation, ρ , was therefore set to zero, and all peaks were symmetric Lorentzians.

Sequence #2 — Datasets in this sequence were comprised of modes from $l = 0$ all the way up to $l = 5$. But, like Sequence #1, there was no correlation of the excitation, or correlation with the granulation-like noise (so, again, $\rho = 0$ and all peaks were again symmetric).

Sequence #3 — Datasets in this sequence were comprised of modes from $l = 0$ to 3, with *no* $l = 4$ and 5 modes. However, correlation of the excitation, and correlation with the granulation-like noise background, was included. The coefficient of correlation was given the same value as the hare-and-hounds dataset, i.e., $\rho = -0.36$. The mode peaks were therefore asymmetric.

Sequence #4 — Datasets in this sequence had the same underlying parameters as the hare-and-hounds dataset, i.e., modes up to $l = 5$, and correlations fixed by $\rho = -0.36$ (so the mode peaks were asymmetric).

The hare then applied a standard (i.e., pair-by-pair) peak-bagging code to the frequency power spectrum of each dataset. This standard code fitted modes a pair at a time, and did not account for the $l = 4$ and 5 modes, or outlying power from modes outside the fitting windows.

Figs. 5 and 6 plot differences between the fitted and input $l = 0$ and $l = 1$ frequencies, respectively, of all four sequences.

We selected these degrees to show the impact on the even- l and odd- l pair fits, respectively. Results on individual datasets in each sequence are rendered in grey; the dark solid lines show the average frequency differences for each sequence, while the dotted lines bound the 1σ standard deviations on these average differences.

The standard peak-bagging code evidently does a good job of recovering the input frequencies when it is presented with the Sequence #1 data (upper left-hand panels of Figs. 5 and 6). There are no $l = 4$ and 5 modes to give problems for the fits; and because there are no correlations in the data, all mode peaks are symmetric. Furthermore, even though the fitting did not take account of outlying power from all other modes, the results were not affected adversely. We shall come back to this point below (discussion of Fig. 7), where we show that matters are not so simple when the mode peaks are asymmetric.

We draw an important conclusion from the Sequence #1 results: provided the mode peaks are symmetric, failure to include power from outlying modes [source (ii)] *will not* bias the estimated frequencies.

The upper right-hand panels of Figs. 5 and 6 show the results for Sequence #2. These datasets now included the $l = 4$ and 5 modes, but, again, peaks were symmetric. The $l = 0$ frequencies are seen to be biased, because the standard peak-bagging failed to take account of power from the newly introduced $l = 4$ and 5 modes. The $l = 1$ frequencies remained unaffected, because the $l = 4$ and 5 modes did not give a significant contribution to the power spectral density in their fitting windows. So, we may draw another important conclusion, this time from the Sequence #2 results: failure to account for power from the $l = 4$ and 5 modes [source (i)] will bias estimates of even- l frequencies. The size of this bias will depend on the visibilities of the $l = 4$ and 5 modes, relative to their more prominent $l = 0$ and 2 counterparts, and the width in frequency of the fitting windows (wider windows will admit more power from the $l = 4$ and 5 modes). For the typical standard peak-bagging scenario tested here – even- l fitting windows were $48\text{-}\mu\text{Hz}$ wide – bias was present in the range ≈ 2.2 to ≈ 3.4 mHz. On average, the bias reached sizes comparable to the estimated frequency uncertainties. However, in some isolated cases (see individual fits shown as grey curves) the bias could be up to three-times as large as the uncertainties.

Similar results were given for fitting window widths of between 40 and $50\text{-}\mu\text{Hz}$ (the range covered by the ten hounds). If the windows are made any narrower – the simplest approach to reducing the impact of the $l = 4$ and 5 modes – a new bias is introduced. This bias appears because the windows are then too narrow to get robust estimates of the falling power in the wings of the mode peaks. If the windows are instead made wider, the impact of the $l = 4$ and 5 modes on the fitted frequencies becomes more severe. For example, when fitting windows were widened to $70\text{-}\mu\text{Hz}$, the bias reversed sign above ≈ 2.5 mHz, and was found to be more than four-times as large as the bias given with $40\text{-}\mu\text{Hz}$ windows.

Let us now turn to the Sequence #3 and Sequence #4 datasets, which both included the effects of correlations and therefore had asymmetric mode peaks. Results from the Sequence #3 data (lower left-hand panels of Figs. 5 and 6) show biased $l = 0$ and $l = 1$ frequencies. The Sequence #3 datasets contained no $l = 4$ and 5 modes, so the source (i) bias could not have been a factor. Rather, it is the source (ii) bias that now comes into play. In summary: failure to account for the power due to modes outside the fitting windows matters when the peaks were asymmetric. Recall it did not matter when the peaks were symmetric (see discussion on Sequence #1 above). To help explain these conclusions, consider Fig. 7.

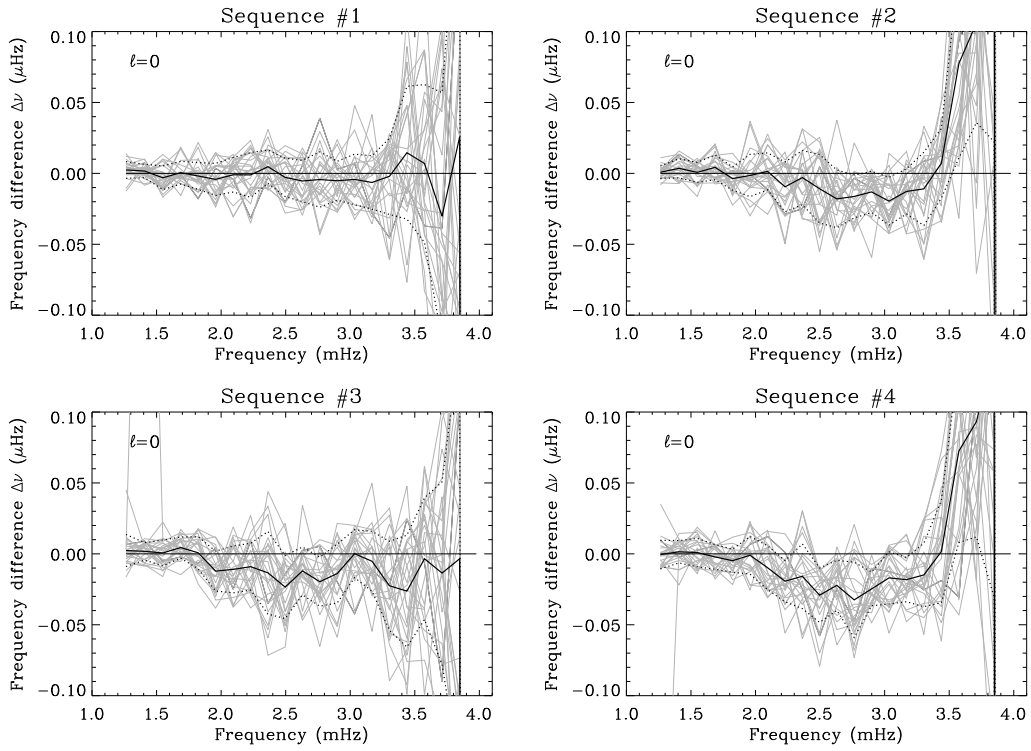


Figure 5. Differences between the fitted and input $l = 0$ frequencies, for fits to the four sequences of artificial solarFLAG datasets (see text for details).

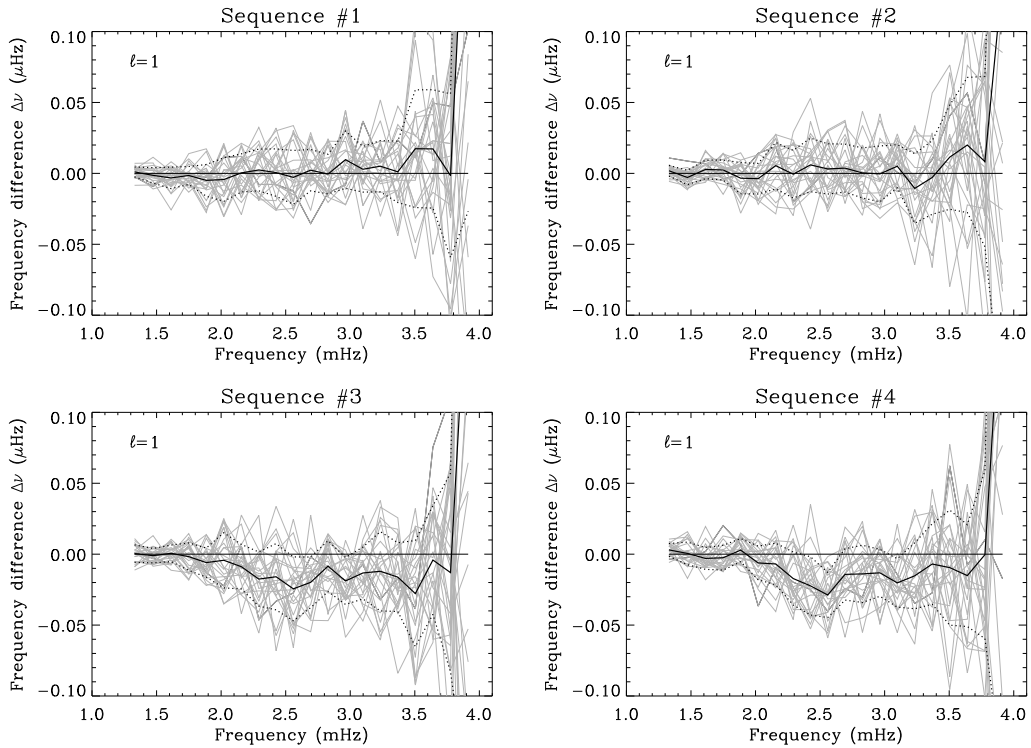


Figure 6. Differences between the fitted and input $l = 1$ frequencies, for fits to the four sequences of artificial solarFLAG datasets.

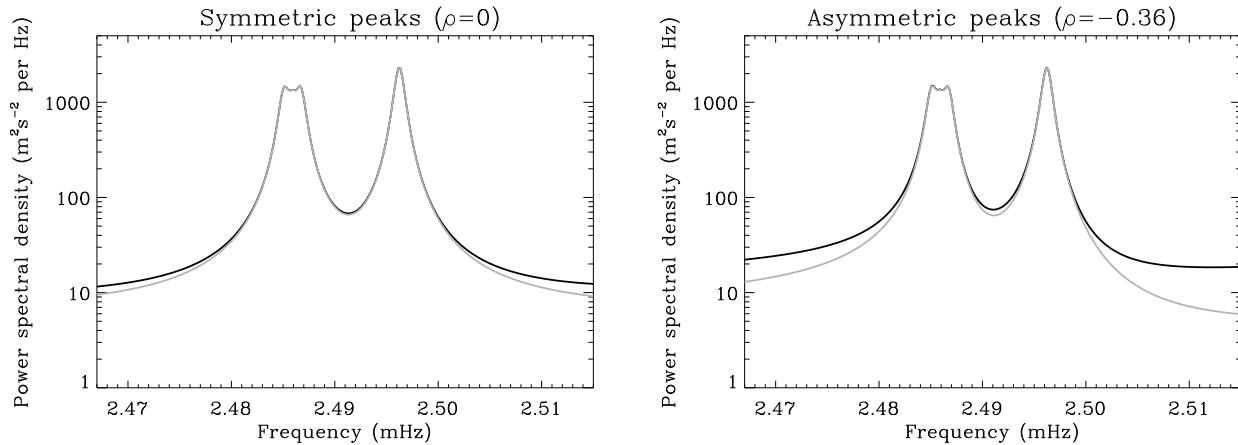


Figure 7. The black curves show the limit frequency power spectra of Sequence #1 (left-hand panel) and Sequence #3 (right-hand panel), in the region of an $l = 2$ (2.486 mHz), $l = 0$ (2.496 mHz) mode pair. The grey curves show the power spectral density due only to the displayed $l = 2$ and 0 mode pair, and the background noise.

The panels in this figure each show the limit frequency power spectrum (black curves) for a different scenario. The left-hand panel shows the limit spectrum for the case of Sequence #1, where all peaks are symmetric Lorentzians. The right-hand panel shows the limit spectrum for the case of Sequence #3, where the introduction of correlations made the peaks asymmetric. The same narrow range in frequency has been chosen for both plots. This range corresponds to the frequency fitting window that would be selected to perform a standard (pair-by-pair) fit to the $l = 2$ (left-hand mode), $l = 0$ (right-hand mode) pair shown.

We recall that in the standard fitting approach, the fitting model includes only power from the mode pair in the chosen window (plus a background term). The grey curve in each panel of Fig. 7 shows this power, i.e., the power spectral density due only to the displayed modes and the background noise. The obvious shortcoming of the standard fitting approach is then made apparent by comparing the black and grey curves in both panels: one is attempting to fit the full spectrum (black curve) using a fitting model which is instead correctly represented by the grey curve.

The difference between the black and grey curves in either panel of course gives the contribution of power from the outlying modes [i.e., source (ii)]. We see that for Sequence #1 the curves are indistinguishable in the immediate neighbourhood of the peaks. Furthermore, the mismatch of power further out looks very similar at the low- and high-frequency ends of the window. We might therefore expect standard fitting estimates of the frequencies from Sequence #1 to not be affected significantly by failing to model the outlying power; and this is of course what we saw in the Sequence #1 fitting results (see above).

Mismatches in power for the asymmetric Sequence #3 data are, in contrast, very evident in the vicinity of the peaks. Furthermore, the mismatches have different sizes at the low- and high-frequency ends of the window. This presents problems for the standard peak-bagging, which tries to fit the black curve to a model comprising only the two displayed modes (plus background), when it is of course the *grey curve* that actually describes the power of displayed modes.

There is more power in the grey curve at the low-frequency end of the window compared to the high-frequency end, because the modes have negative asymmetry. However, that difference in power is less pronounced in the black curve. Attempts to fit the

black curve to a model comprising the two modes will therefore tend to return estimates of the asymmetry that are smaller, and less negative, than the true asymmetry, the latter seen in the shape of the grey curve. (Note that the best-fitting estimate of the observed power will be close to the black curve.) The estimated asymmetries will therefore be positively biased. This will in turn lead directly to negative bias in the estimated frequencies.

These conclusions are borne out by checking the fitted asymmetries, and fitted frequencies, of the Sequence #3 results. The predicted positive bias is present in both the $l = 0$ and $l = 1$ asymmetry estimates (see also Fig. 4). Furthermore, we see the expected (highly significant) anti-correlation between bias in the asymmetries and bias in the frequencies.

We may also use the plots in Fig. 7 to explain why two of the hounds who tried to allow for outlying power still obtained frequencies that were biased. Both hounds modelled the outlying power in terms of symmetric Lorentzians, while the hare-and-hounds data of course contained asymmetric mode peaks. The left-hand panel of Fig. 7 shows that modelling the outlying power in this way will lead to only fairly modest changes in the power spectral density. We would therefore have expected the “outlying” power in the two hounds’ fitting models to have made little difference in fits to asymmetric hare-and-hounds data. Looking at the right-hand panel of Fig. 7, their model representations of the two modes plus outlying power would have been little different to the grey curve; and so the estimated frequencies remained biased.

We draw perhaps the most important conclusion of the paper from the Sequence #3 results: failure to account for power from modes whose central frequencies lie outside the fitting windows will bias estimates of both the even- l and odd- l frequencies, above ≈ 1.8 mHz, by an amount that, on average, can again reach the size of the typical frequency uncertainties. In some isolated cases (see individual fits shown as grey curves) the frequency bias may be up to three-times as large as the uncertainties.

Finally, the Sequence #4 results (lower right-hand panels of Figs. 5 and 6) bring everything together, and show the total impact of our two main sources of bias. Recall these datasets contained $l = 4$ and 5 modes, and correlations, and as such they had the same underlying properties as the hare-and-hounds dataset. The results demonstrate that the total frequency bias is on average most significant in the estimated $l = 0$ frequencies, because source (i) and

source (ii) give a similar-sized contribution to the bias. In some isolated cases (again, see the grey curves) the total bias may be almost four-times the size of the frequency uncertainties. The bias is on average less severe in the $l = 1$ results, because only the source (ii) bias plays a significant rôle in affecting the odd- l pair fits.

6 SUMMARY AND CONCLUDING DISCUSSION

We have used the new solarFLAG simulator, which includes the effects of correlated mode excitation and correlations with background noise, to make artificial timeseries data that mimic Doppler velocity observations of the Sun as a star. The correlations give rise to asymmetry of mode peaks in the frequency power spectrum.

A 3456-day dataset was used as the input data for the latest solarFLAG hare-and-hounds exercise. This paper reports on the results of that exercise, which was concerned with testing methods for extraction of p-mode frequencies of low-degree (low- l) modes. Ten hounds applied their peak-bagging codes to the hare-and-hounds dataset. Peak-bagging involves maximum-likelihood fitting of mode peaks in the frequency power spectrum to multi-parameter fitting models. Each hound returned peak-bagging estimates of the frequencies of the artificial $l = 0$ to 3 modes to the hare (who was WJC) for further scrutiny.

Analysis of the results showed clear evidence of a systematic bias in the estimated frequencies of modes above ≈ 1.8 mHz. The bias is negative, meaning the estimated frequencies systematically underestimate the input frequencies. A follow-up analysis on independent realizations of the hare-and-hounds dataset showed that in some fits the bias could be as much as three- to four-times as large as the frequency uncertainties. Over the affected range of mode frequencies, the average bias is typically one to two-times the frequency uncertainties.

We identified two sources that are the dominant contributions to the frequency bias. Both sources involve failure to model accurately subtle aspects of the observed power spectral density in the part (window) of the frequency power spectrum that is being fitted. One source of bias arises from a failure to account for the power spectral density of the weak $l = 4$ and 5 modes. The other source arises from a failure to account for the power spectral density coming from all those modes whose frequencies lie outside the fitting windows (“outlying” power).

The main lesson to be drawn from this paper is that the Sun-as-a-star peak-bagging codes need to allow for both sources, otherwise the frequencies given by analysis of real Sun-as-a-star data will in all likelihood be biased. The identification, and measurement, of the bias from “outlying” power is the most important new finding of the paper. Can we afford to ignore its effects? The short answer must be no. Our analysis suggests the magnitude of its frequency bias may be up to three-times as large as the frequency uncertainties, depending on the impact of realization noise, and it could present problems for helioseismic inference on the solar structure from inversions of the mode frequencies.

The precise sizes of biases given on the real Sun-as-a-star data will clearly depend on how closely our artificial data resemble those real data. We are certainly now able to reproduce frequency power spectra that bear a close resemblance to the real spectra – courtesy of the new solarFLAG simulator – and this suggests our bias estimates do have quantitative merit where helioseismic predictions concerning the real data are concerned. However, we should bear in mind that there may be some aspects of the real Sun-as-a-star data that are not reproduced exactly in the artificial data.

One such detail concerns the exact shapes shown by the asymmetric mode peaks. In the real solar p-mode data, it is assumed that there is also a contribution to the asymmetry owing to the radial location, extent, and multipole properties, of the acoustic sources. The question then arises: Is the underlying form of the power spectral density due to these contributions the same as that from the correlated noise modelled in the solarFLAG simulator? Subtle differences would affect the sizes of the frequency biases.

We finish with a few comments on implications of the results of this paper for the peak-bagging codes. The standard Sun-as-a-star approach is to go through the frequency power spectrum fitting a pair of modes at a time. For such an approach to be useful our results here stress the need for power from the outlying modes to be fully accounted for in the fitting windows (so-called “pseudo whole-spectrum” fitting). The other option is to fit all modes in the frequency power spectrum in one go (so-called “whole spectrum” fitting). Either way, it is not sufficient to have an approximate, or first-order, estimate of the outlying, or total, power spectral density: the estimate must be very accurate, otherwise the frequency bias will remain, or additional bias may be introduced.

In order to provide such an estimate, it is necessary to describe accurately the power spectral density of each mode peak a long way from its resonant frequency (i.e., in the decaying wings of the peaks). The fitting formalism most often used to model the asymmetric power spectral density of the mode peaks – that due to Nigam & Kosovichev (1998) – fails in such a description. This is because the Nigam & Kosovichev formalism is an approximation (low-order expansion) that is usable only at frequencies close to resonance. Far from resonance, the modelled power spectral density tends to a constant offset not shown by the real data³

Clearly the requirements on the sought-for fitting model are that it should describe the asymmetric peaks both close to resonance, and far from resonance where we know the power falls off significantly in the real p-mode peaks. There is, potentially, a very simple solution to this problem. If the high-order terms in the Nigam & Kosovichev formalism (those in the square of the asymmetry parameter) are disregarded, it turns out that the resulting, truncated formalism can satisfy both of the above requirements. Indeed, it has the correct form to model accurately the asymmetric shapes given by correlated noise (see Toutain, Elsworth & Chaplin 2006). The issue then arises as to whether this is sufficient to describe the shapes of the real p-mode peaks (see previous comments above). Another approach is to generate a model of resonant spectrum in one go, with all the overtone structure included, rather than model the spectrum as a superposition of individual Lorentzian-like peaks. This may be accomplished using a suitable form for the acoustic potential of the solar cavity, together with information on the acoustic source and the reflection and transmission properties of the upper cavity boundary (e.g., see Jefferies, Vorontsov & Giebank 2004).

Finally, we note that the detailed conclusions drawn in this paper are for the Sun-as-a-star observations. The Sun-as-a-star techniques are of course also directly applicable to stars that show Sun-like oscillations, and we are now starting to get *asteroseismic* peak-bagging results on other stars (e.g., see Fletcher et al. (2006), who analyzed data collected by WIRE on α Cen A; and Appourchaux et al. (2008), who have analyzed the first Sun-like oscillations data collected by CoRoT, on the star HD49933). A peak-

³ The “Fano profile” formula in Gabriel et al. (2001) also fails in this regard, because it retains those terms that lead to the offset far from resonance.

bagging pipeline is being constructed by the asteroFLAG group⁴ (Chaplin et al. 2008a) for application to the asteroseismic data that will be collected on hundreds of Sun-like stars by the NASA Kepler mission (Christensen-Dalsgaard 2007). Even though the intrinsic signal-to-noise ratios will be lower than for the Sun-as-a-star data some stars will be monitored continually for several years, meaning we should be able to constrain the p-mode parameters to high levels of precision. With the p-mode parameters reflecting different intrinsic properties of the stars, we should expect to be confronted with many different potential bias problems in different parts of the color-magnitude diagram occupied by the Sun-like oscillators (Appourchaux et al. 2006a, b; Chaplin et al. 2008b). Similar studies to the one undertaken here for the Sun as a star are now being made by asteroFLAG to prepare the peak-bagging analysis for Kepler.

ACKNOWLEDGMENTS

WJC and SJJ-R acknowledge the support of STFC. This work was also supported by the European Helio- and Asteroseismology Network (HELAS), a major international collaboration funded by the European Commission's Sixth Framework Programme. WJC also thanks Sarbani Basu and Aldo Serenelli for providing the model BS05(OP) frequencies.

REFERENCES

- Appourchaux T., 2003, *Ap&SS*, 284, 109
- Appourchaux T., Berthomieu G., Michel E. et al, 2006a, in *The CoRoT Mission*, A. Baglin, J. Lochard, M. Fridlund, L. Conroy eds., Publication ESA SP-1306, p. 429
- Appourchaux T., Berthomieu G., Michel E. et al, 2006b, in *The CoRoT Mission*, A. Baglin, J. Lochard, M. Fridlund, L. Conroy eds. Publication ESA SP-1306, p. 377
- Appourchaux T., et al., 2008, *A&A*, submitted
- Bahcall, J. N., Serenelli, A. M., & Basu, S. 2005, *ApJ*, 621, L85
- Barban C., Hill F., Kras S., *ApJ*, 2004, 602, 516
- Chaplin W. J., Elsworth Y., Isaak G. R., McLeod C. P., Miller B. A., New R., 1997, *MNRAS*, 287, 51
- Chaplin W. J., et al., 2006, *MNRAS*, 369, 985
- Chaplin W. J., Elsworth Y., Toutain T., 2008, *AN*, 329, 440
- Chaplin W. J., et al., 2008a, *AN*, 329, 549
- Chaplin W. J., Houdek G., Appourchaux T., Elsworth Y., New R., Toutain T., 2008b, *A&A* (arXiv:0804.4371)
- Christensen-Dalsgaard J., 1989, *MNRAS*, 239, 977
- Christensen-Dalsgaard J., Arentoft T., Brown T. M., Gilliland R. L., Kjeldsen H., Borucki W. J., Koch D., 2007, *CoAst*, 150, 350
- Fletcher S. T., Chaplin W. J., Elsworth Y., Schou J., Buzasi D., 2006, *MNRAS*, 371, 935
- Fletcher S. T., Chaplin W. J., Elsworth Y., New R., 2008, *AN*, 329, 447
- Gabriel A. H., Connerade J. P., Thiery S., Boumier P., 2001, *A&A*, 380, 745
- Gelly B., et al., 2002, *A&A*, 394, 285
- Harvey J., 1985, in: *Future missions in solar, heliospheric and space plasma physics*, eds. E. Rolfe, B. Battrock, ESA SP-235, Noordwijk, Netherlands, p. 199
- Jefferies S. M., Severino G., Moretti P.-F., Oliviero M., Giebinck C., 2003, *ApJ*, 596, L67
- Jefferies S. M., Vorontsov S. V., Giebinck C., 2004, in: *Helio- and Asteroseismology: Towards a Golden future*, SOHO14/GONG 2004, ed. D. Dansey, ESA-559, New Haven, USA, p. 254
- Jiménez A., Roca-Cortés T., Jiménez-Reyes S. J., 2002, *SolPhys*, 209, 247
- Lazrek M., Gelly B., Grec G., Renaud C., Fossat E., in: *Helio- and Asteroseismology at the Dawn of the New Millennium*, Proc. SOHO 10/GONG 2000, Tenerife, Spain, ed. A. Wilson, ESA SP-464, Noordwijk, Netherlands, p. 523
- Nigam, R., & Kosovichev, A. G. 1998, *ApJ*, 505, L51
- Roxburgh I. W. & Vorontsov S. V., 1997, *MNRAS*, 292, L33
- Severino G., Magrì M., Oliviero M., Straus Th., Jefferies S. M., 2001, *ApJ*, 561, 444
- Toutain T., Elsworth Y., Chaplin, W. J., 2006, *MNRAS*, 371, 1731

⁴ <http://www.issibern.ch/teams/Astflag>